The Reactivity of Hydrogen Enriched Turbulent Flames

F. Hampp[a,b], K. H. H. Goh[a], R. P. Lindstedt[a,*]

[a] *Department of Mechanical Engineering, Imperial College, London, SW7 2AZ, UK*
[b] *German Aerospace Center (DLR), Institute of Combustion Technology, Stuttgart 70569, Germany*

Abstract

The use of hydrogen enriched fuel blends, e.g. syngas, offers great potential in the decarbonisation of gas turbine technologies by substitution and expansion of the lean operating limit. Studies assessing explosion risks or laminar flame properties of such fuels are common. However, there is a lack of experimental data that quantifies the impact of hydrogen addition on turbulent flame parameters including burning velocities and scalar fluxes. Such properties are here determined for aerodynamically stabilised flames in a back-to-burnt opposed jet configuration featuring fractal grid generated multi-scale turbulence ($Re_t = 314 \pm 19$) using binary H_2 / CH_4 and H_2 / CO fuel blends. The binary H_2 / CH_4 fuel blend is varied from $\alpha = X_{H2}/(X_{H2} + X_F) = 0.0$, 0.2 and 0.4 – 1.0, in steps on 0.1, and the binary H_2 / CO fuel blend from $\alpha = 0.3$ – 1.0 also in steps of 0.1. The equivalence ratio is adjusted between the mixture specific lower limit of local flame extinction and the upper limit of flashback. The flames are characterised using PIV measurements combined with a flame front detection algorithm. The study quantifies the impact of hydrogen enrichment on (i) turbulent burning velocity (S_T), (ii) turbulent transport and (iii) the rate of strain acting on flame fronts. Scaling relations (iv) that correlate S_T with laminar flame properties are evaluated and (v) flow field data that permits validation of computational models is provided. It is shown that CH_4 results in a stronger inhibiting effect on the reaction chemistry of H_2 compared to CO, that turbulent transport and burning velocities are strongly correlated with the rate of compressive strain and that scaling relationships can provide reasonable agreement with experiments.

Keywords: Hydrogen, Turbulent Premixed Combustion, Syngas, Turbulent Burning Velocity, Scalar Transport, Rate of Strain

*Corresponding author. Tel: +44 20 7594 7039; *Email:* p.lindstedt@imperial.ac.uk

1. Introduction

The confluence of climate change, environmental protection and diminishing fossil fuel resources have promoted the development of low carbon footprint and clean energy technologies [1]. State-of-the-art gas turbines operate under fuel lean conditions optimised for natural gas [2] and single digit nitrogen oxide emissions have been achieved. The use of hydrogen enriched fuel blends, e.g. syngas, offers great potential in the decarbonisation of related technologies by substitution and expansion of the lean operating limit [3]. Decarbonisation by means of hydrogen substitution is most effective if hydrogen is produced from renewable energy sources. However, the variability of syngas compositions can lead to fuel flexibility problems for manufacturers [4] and the increased hydrogen concentration to safety concerns [5]. The syngas mixture reactivity is strongly dependent upon hydrogen content with direct implications on flame propagation speeds, explosion over-pressures, auto-ignition and turbulence–chemistry interactions. The latter can lead to differences in flame surface area [6] and combustion instabilities [1, 4]. Li et al. [5] measured flame speeds and over-pressures generated in an obstructed flame tube for a wide range of binary and ternary H_2, CO and CH_4 mixtures, with methane showing a stronger inhibiting effect on the mixture reactivity. Scaling based on the amount of air required to fully oxidise the mixture correlated the fuel composition impact on explosion over-pressures [5] and turbulent flow fields [7]. Simatos *et al.* [8] investigated the effect of H_2 content in lean ($\Phi = 0.80$) binary CH_4 and CO fuel blends on auto-ignition in turbulent shear layers and the stronger inhibiting effect of CH_4 prevailed.

The turbulent burning velocity (S_T) is a key parameter required, for example, to evaluate the strength of explosions [5] and the flashback propensity in gas turbine engines [9]. Investigations seeking to correlate S_T to the turbulence intensity are quite common [10]. Wang *et al.* [11] investigated the effect of hydrogen content on S_T and explored scaling relations under gas turbine relevant conditions, and found that H_2 addition alters the correlation due to preferential diffusive-thermal effects [2]. Scaling relations for the turbulent consumption speed of H_2 /CO mixtures can include flame stretch and pressure effects as shown by Venkateswaran *et al.* [12] for a wide range of conditions. Shy *et al.* [13] evaluated the effect of turbulent Reynolds (Re_t), Damköhler (Da) and Karlovitz (Ka) numbers for lean syngas flames. Zhang *et al.* [14] evaluated a Kobayashi type turbulent burning velocity correlation for mixtures including H_2 / CO blends with reasonable agreement. Daniele *et al.* [15] showed a linear correlation of S_T with equivalence ratio and inlet bulk velocity for various syngas related mixtures. The impact of hydrogen blending on methane was found to be particularly prominent under ultra-lean conditions. The Lewis number effect on S_T was also found to be significant in binary H_2 / CH_4 and propane mixtures [16] and the effect of pressure was investigated by Liu *et al.* [17]. Multiple turbulent burning velocity definitions (e.g. Bray [18]) have been advanced and Driscoll [19] has shown that the definitions of Shepherd and Cheng [20] and Lawn and Schefer [21] are not equivalent. Yet, the S_T definitions of Bray [18], Lawn and Schefer [21] and a variant proposed by Driscoll [19] agree within $\pm$ 20% for some premixed twin opposed jet flames [22]. However, a broader understanding of the impact of mixture reactivity on turbulent flame propagation is lacking. An

additional difficulty is that theories for premixed flames with a $Da \simeq 1$ are not well developed in contrast to the corrugated flamelet regime ($Da \gg 1$). The current study provides an extensive data set that establishes the impact of fuel reactivity on S_T at $Da \simeq 1$ to support the removal of such limitations.

The opposed jet configuration provides a canonical geometry with distinct advantages for the assessment of fuel effects [23]. The geometry features aerothermochemistry related flame stabilisation [24], essentially adiabatic conditions [25], comparatively well developed turbulence [26], excellent optical access [27] and accurate control of boundary conditions [23]. The turbulent to bulk strain ratio can be substantially increased without bulk flow instabilities [23] via the use of cross fractal grids (CFGs) [26]. The back-to-burnt (BTB) configuration further allows the stabilisation of flames at low Damköhler numbers and permits investigations of combustion regime transitions [24, 28]. In particular, self-sustained flames detach from the stagnation plane and become independent of the opposing burnt gas [29], while low Da combustion is dominated by interactions between the two streams [30, 31].

The current study is using Particle Image Velocimetry (PIV) and a flame front detection algorithm [23, 29] to quantify the impact of H_2 enrichment on CH_4 and CO fuel blends by determining the impact on (i) turbulent burning velocities (S_T), (ii) turbulent transport and (iii) the rate of strain acting on flame fronts. Scaling relations (iv) that correlate S_T with laminar flame properties are evaluated and (v) flow field data for validation of computational fluid mechanics (CFD) based models for risk assessment is provided.

2. Experimental configuration

The present opposed jet configuration was originally developed by Geyer *et al.* [27] and has been used by Geipel *et al.* [26], Goh *et al.* [22, 25] and Hampp and Lindstedt [24, 29, 30, 32]. A schematic is provided in Fig. 1. The burner consists of two identical nozzles with an inner diameter $D =$ 30 mm, nozzle length of $L = 50$ mm and nozzle separation of one D. The burner is operated in a back-to-burnt (BTB) configuration to accommodate the wide range of mixture reactivities. The configuration entails considerable advantages in the current context: (i) cases can be compared on a basis of nearly identical flow conditions [29], (ii) all fuel gases are combusted (a safety requirement for H_2 and CO containing mixtures) [5] as global extinction is prevented, (iii) the transition from self-sustained flame propagation to thermally supported burning can be assessed [24] and (iv) self-sustained flames detach from the stagnation plane with combustion dynamics related to the intrinsic aerothermochemistry. A purpose written LabView interface is used to control the Bronkhorst mass flow controllers with a maximum uncertainty of $\pm$ 0.5% of full scale. All gases are supplied at a pressure of 4.0 bar(g) with the upper nozzle air seeded with ~ 3 μm Al_2O_3 particles [25].

2.1. Flow conditions

In order to determine the impact of fuel reactivity on turbulent burning velocities and scalar transport, the binary H_2 / CH_4 and H_2 / CO fuel blends are varied from $\alpha = X_{H2}/X_F = 1.0$, 0.9, 0.8, 0.7, 0.6, 0.5, 0.4, 0.2 and 0 and 1.0, 0.9, 0.8, 0.7, 0.6, 0.5, 0.4 and 0.3, respectively, where X is the fuel mole

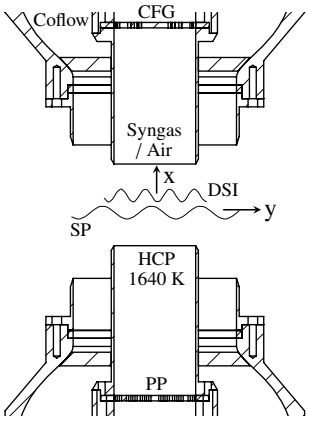

Figure 1: Schematic of the back-to-burnt opposed jet burner configuration. CFG – cross fractal grid, DSI – density segregation iso-contour, SP – stagnation plane, (x,y) – coordinate system, HCP – hot combustion products, PP – perforated plate.

fraction in the blend and F the blending component (i.e. CH_4 or CO). The mixture compositions are listed in the supplementary material. The premixed fuel / air mixtures are injected through the upper nozzle with a constant bulk velocity of $U_b = 9.0$ ms^{-1} and a reactant temperature of $T_r = 298$ K. A cross fractal grid (CFG) is used to provide a well developed multi-scale turbulent flow with enhanced intensity [22]. The flow is maintained constant with an integral length scale of turbulence of $L_I = 3.9 \pm 0.2$ mm [30]. Velocity fluctuations at the nozzle exit of $u_{rms} = 1.4 \pm 0.1$ ms^{-1} are measured using PIV. The turbulent Reynolds number ($Re_t = L_I \cdot u_{rms}/\nu_r = 314 \pm 19$) is modestly affected by fuel composition changes, primarily due to the kinematic viscosity of the reactants (ν_r). The turbulent kinetic energy dissipation rate in the reactants is determined as $\epsilon_r = u_{rms}^3 L_I^{-1} \simeq 700$ m^{2}s^{-3}.

The lower nozzle hot combustion products (HCP) are generated from lean ($\Phi = 0.60$) premixed 50% H_2 / 50% CH_4 flames stabilised on a perforated plate. The HCP are in close-to thermochemical equilibrium with a nozzle exit

temperature of 1640 ± 7.1 K measured using a 50 μm R-type thermocouple. The HCP composition, including the residual oxygen concentration, does not exert a strong impact on the self-sustained flames [28, 30, 31] of primary interest here.

2.2. Diagnostic setup

The flow field is measured by PIV using a double pulse Nd:YAG laser. The laser sheet thickness is estimated to ~ 0.3 mm using burn marks with an optimum time delay between pulses of $\Delta t = 25$ μs. The interrogation region of 40 $\times$ 30 mm is resolved by 1376 $\times$ 1040 pixels using a CCD-camera. A 100 mm Nikon lens is equipped with a 99% neutral density and a 3 nm bandpass filter centred at 532 nm to minimise noise. The PIV vectors are calculated via a multi-pass cross-correlation with decreasing window size resulting in a spatial vector resolution of 0.90 mm and vector spacing of 0.45 mm. For each set of conditions, 1000 double frame images are recorded to assure statistically independent data. The relaxation time (τ_p) of the 3 μm Al_2O_3 seeding particles is estimated to $\tau_p = 107$ μs which is similar to the smallest PIV timescale of 102 μs. The Stokes number ($St = \tau_p/\tau_\eta$) is determined to $St \simeq 0.75$ based on a Kolmogorov timescale of $\tau_\eta \simeq 156$ μs. Out-of-plane, out-of-pattern, beam steering and uncertainties due to thermal gradients are negligible [24, 29].

3. Data analysis

The following section introduces the utilised scaling relations, evaluated turbulent flame properties and uncertainty analysis.

3.1. Reaction progress and scalar transport

A conventional PIV particle based density segregation technique is used to detect the instantaneous flame front [23, 33]. The accuracy of the algorithm was evaluated by Hampp and Lindstedt [24] and found to deviate less than two Kolmogorov length scales from the 600 K iso-contour (e.g. Schlieren contour). The turbulent flame brush and the reaction progress variable ($\overline{c}$) are determined from the statistical location of the instantaneous flame front (c_i), while the measured turbulent burning velocity ($S_{T,l}$) is determined based on the leading edge ($\overline{c} = 0.02$) [21]. The scalar flux is evaluated as $\overline{c'u'} = \overline{c} \cdot (1 - \overline{c}) \cdot \overline{U_s}$, where the slip velocity is defined as the difference between product and reactant fluid velocities, i.e. $\overline{U_s} = \overline{U_p} - \overline{U_r}$ [34].

3.2. Conditional rate of strain

The normal rate of strain conditioned on the instantaneous flame front is calculated using the methodology of Hampp and Lindstedt [29, 30]. The instantaneous planar strain rate tensor ($e_{ij} = 0.5(\partial u_i/\partial x_j + \partial u_j/\partial x_i)$) is calculated from the PIV data. The normal ($a_n = f_{11}$) strain component is determined by $f = \mathbf{R}(\Theta) \cdot e$, where $\mathbf{R}$ is the rotation matrix and Θ is the angle between the iso-contour normal and the theoretical stagnation point streamline (SPS). The analysis includes the stagnation point movement in the radial limit $\pm$ 0.5 L_I away from the SPS [26]. Correlations with mean values of the conditional normal compressive strain ($\overline{a_n}$) are discussed below.

3.3. Scaling relations for mixtures with high H_2 content

The wide range of H_2 concentrations results in significant differences in the mixture reactivity as well as reactant and burning properties. Li *et al.* [5, 7]

presented a scaling factor for fuel lean blends of H_2 with CH_4 and CO defined based on the amount of air required to fully oxidise each fuel component ($0 \leq \beta \leq 1$). The β factor improved the scaling of explosion over-pressures and related flow velocities compared to α ($= X_{H2}/(X_{H2} + X_F)$) for a wide range of binary and ternary H_2 / CH_4 / CO mixtures. The scaling of auto-ignition in a turbulent shear layer was also improved [8] and β (see Eq. (1), where $(X_k/X_A)_{st}$ is the stoichiometric fuel air ratio) is used here.

$$\beta = \left(\frac{X_{H2}}{(X_{H2}/X_A)_{st}}\right) / \left(\frac{X_{H2}}{(X_{H2}/X_A)_{st}} + \frac{X_F}{(X_F/X_A)_{st}}\right) \tag{1}$$

3.4. Turbulent burning velocity scaling relationships

Classical theories for turbulent combustion resulting in eddy breakup based models for the reaction rate source term (e.g. [35]) only provide a scaling of the turbulent burning velocity based on the (isotropic) velocity fluctuations (e.g. u') as shown via Kolmogorov, Petrovskii and Piskunov (KPP) [36] or eigenvalue [37] analyses. The velocity fluctuations are kept constant in the current study to isolate the impact of the mixture reactivity. The classical form for expressing the turbulent burning velocity is:

$$\frac{S_T}{S_L} = 1 + c\left(\frac{u'_l}{S_L}\right)^m \text{ with } 0.5 \leq m \leq 1 \tag{2}$$

Examples of correlations (e.g. [10, 11, 13, 14]) for S_T from Zhang *et al.* [14] ($S_T^{\#}$), Bradley *et al.* [38] ($S_T^{\ddagger}$) and Peters [39] ($S_T^{\dagger}$) are given in Eq. (3),

$$\frac{S_T^{\#}}{S_L} = 2.92\left(\frac{u_l'}{S_L}\right)^{0.55}$$
$$\frac{S_T^{\ddagger}}{S_L} = \frac{0.88}{(KLe_r)^{0.3}}\left(\frac{u_l'}{S_L}\right) \text{ where } K = 0.157\left(\frac{u_l'}{S_L}\right)^2 Re_t^{-1/2} \quad (3)$$
$$\frac{S_T^{\dagger}}{S_L} = 1 - \frac{\psi L_I}{4\delta_f} + \left[\left(\frac{\psi L_I}{4\delta_f}\right)^2 + \psi\frac{u_l' L_I}{S_L \delta_f}\right]^{\frac{1}{2}}$$

In Eq. (3), $\psi = 0.78$, u_l' is the axial velocity fluctuation at the leading edge, δ_f the laminar flame thickness, K the Karlovitz stretch factor and Le_r the Lewis number (ratio of Schmidt and Prandtl numbers) of the reactants. The expression for Le_r is given in Eq. (4) and assumes that the deficient reactant is the dominant fuel component for the current fuel lean mixtures.

$$Le_r = \frac{X_{H_2} Le_{H_2} + X_F Le_F}{X_{H_2} + X_F} \quad (4)$$

A fractal flame front analysis has been used to show that the rate of reaction depends on the ratio of the laminar burning (S_L) and Kolmogorov ($V_\kappa = (\nu_r \epsilon_r)^{1/4}$) velocities [40]. Such forms are evidently more applicable in the current context where fuel reactivity comes to the fore. The applied KPP analysis [41] provides the estimate of the turbulent burning velocity (S_T^*) shown in Eq. (5). The form includes the KPP limit eigenvalue ($\Lambda = 2$), the customary turbulent eddy viscosity $C_\mu = 0.09$ and reaction rate $C_R \simeq 4$ constants [42]. The Le_r correction by Aluri *et al.* [43] gives $C_R = 4.0/e^{Le_r - 1}$.

$$\frac{S_T^*}{S_L} = 1 + \Lambda \cdot \sqrt{\frac{3}{2} C_R \frac{C_\mu}{Sc_t}\frac{S_L}{V_\kappa}} \cdot \left(\frac{u_l'}{S_L}\right) \quad (5)$$

The turbulent Schmidt number (Sc_t) is also required and depends greatly on

the flow configuration. It is typically in the range $0.3 \leq Sc_t \leq 1$ [44] and a common value $Sc_t = 0.7$ is used here. As discussed below, the gradient diffusion hypothesis used to derive Eq. (5) is subject to significant uncertainties. Laizet and Vassilicos [45] have further shown that scalar transport can be significantly enhanced for fractal grids due to the multiscale nature of the generated turbulence. Nevertheless, Goh *et al.* [22, 23] have shown that the above expression can provide reasonable agreement and it was further noted that a modest reduction in Sc_t would bring improved agreement.

3.5. Laminar flame properties required for scaling

The laminar flame data, i.e. unstrained burning velocity ($S_{L,0}$), flame thickness (δ_f) and adiabatic flame temperature (T_{ad}), required for the evaluation of the used scaling relationship, are obtained from freely propagating flame calculations using detailed chemistry with differential diffusion effects included [46]. Li *et al.* [5] validated the chemical mechanism for a wide range of binary fuel mixtures. The inlet conditions of the laminar flame calculations matched the experiment, i.e. $T_r = 298$ K, $P_0 = 1$ atm and species mole fractions. The computational domain is resolved by 550 nodes featuring a mesh size of ~ 10 μm. Reactant mixture properties such as kinematic viscosity (ν_r), density (ρ_r) and Lewis number (Le_r) are also inferred from the calculations. The laminar extinction strain (a_q) is determined by means of counterflow flame calculations. The computational domain of the latter is resolved by 340 nodes with a local resolution of ~ 20 μm in the reaction zone. The rate of strain is increased in steps of 100 s^{-1} until the laminar flames extinguished. The extinction strain is defined as the highest rate of strain prior extinction for each mixture. The strained laminar burning velocity (S_L)

used for the theoretical scaling relations is determined at the bulk strain rate ($a_b = 600$ s^{-1}) matching the experiment. This accounts for the differences in stretch effects on S_L for the wide range of mixture reactivity investigated and improves the predictability of the scaling relations [12]. The calculation results are summarised in Table 1. The data are further used to determine the Damköhler number ($Da = (L_I \cdot S_L)/(u_{rms} \cdot \delta_f)$) as listed in Table 2.

3.6. Uncertainty analysis and data rejection

The flames of interest in the current investigation are within or close-to the thin reaction zone regime. Moreover, the heat release parameter is only weakly dependent on the fuel blending fractions with similar adiabatic flame temperature for a given Φ. Consequently, the effect of the fuel mixture composition on the detected flame front and thus reaction progress variable is negligible for a given stoichiometry. In the range from $\overline{c} = 0.5 \pm 0.1$, i.e. the conditioning variable, the reactant and product fluid velocity changes are $<$ 2.5%. Consequently, a translation of the detected instantaneous iso-contour within the laminar flame thickness has a negligible impact on the measured scalar flux. A translation of the detected instantaneous iso-contour also provides the largest uncertainties in the measured turbulent burning velocities and the turbulence intensity required for the determination of $S_T^{\#}$, $S_T^{\ddagger}$, $S_T^{\dagger}$ and S_T^{*}. Therefore, a sensitivity analysis of the leading edge position (x_l) on S_T and u_l' is conducted in the range from $x_l \pm 0.25 L_I$. The range corresponds to pure mixing dominated reaction progress that provides the lowest gradient in the reaction progress variable and thus a conservative estimate. The turbulent intensity is approximately constant in the proximity of the leading edge with a variation below 3% for the above x_l variation. The effect of x_l

on the measured S_T^* is below 10%. Thus, a shift in the reaction progress variable iso-contour, e.g. due to uncertainties in detection, fuel composition and changes in equivalence ratio, has a modest impact on the determined turbulent burning velocities.

Flame propagation in the BTB configuration can be influenced or governed by the counterflow hot combustion products for cases with insufficient flame detachment from the stagnation plane [30]. This can result in questionable S_T values as the reaction progress may become influenced by auto-ignition events. Accordingly, the mean velocity at the trailing edge ($\overline{u_t}$) of the flame brush (i.e. at $\overline{c} = 0.95$) is evaluated and cases where $\overline{u_t}$ is negative (the flow direction of the HCP) are removed. For such cases the thermal support provided by the HCP can have a significant impact.

4. Results and discussion

4.1. Flow field statistics

An example of unconditional velocity statistics along the theoretical stagnation point streamline is shown in Fig. 2 for the 60% H_2 / 40% CH_4 mixture at $\Phi = 0.50$ and 0.70 and 60% H_2 / 40% CO mixture at $\Phi = 0.45$. An increase in mixture reactivity (e.g. H_2 content or Φ) results in a faster propagating flame that stabilises further upstream. An increase in equivalence ratio further leads to a stronger dilatation. The latter results in an elevated mean axial velocity ($\overline{U}/U_b$) and an earlier and more pronounced peak in the axial velocity fluctuations ($\sqrt{u'u'}/U_b$) [23]. The stronger inhibiting effect of methane on the H_2 reaction chemistry compared to carbon monoxide, that was also observed in turbulent explosions [5, 7] and auto-ignition re-

lated flame stabilisation [8], is readily evident in the unconditional velocity statistics. This can be inferred from Fig. 2, where the unconditional velocity statistics of the 60% H_2 / 40% CO mixture at $\Phi = 0.45$ is distinctly closer to the 60% H_2 / 40% CH_4 mixture at $\Phi = 0.70$ than the $\Phi = 0.50$ flame.

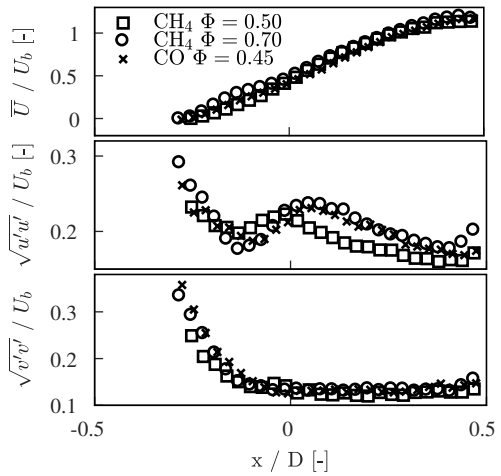

Figure 2: Unconditional velocity statistics ($\overline{U}$ mean axial velocity, u' axial fluctuation, v' radial fluctuation) along the stagnation point streamline, normalised by the bulk velocity (U_b), for the 60% H_2 / 40% CH_4 and 60% H_2 / 40% CO mixtures at different Φ.

The corresponding conditional reactant and product fluid velocity statistics are depicted in Figs. 3 and 4, respectively. The advanced reaction onset for the case with $\Phi = 0.70$ yields an elevated mean axial reactant velocity ($\overline{U_r}/U_b$) in the proximity of $x/D = 0$. As the turbulent flow field is maintained constant, the conditional axial and radial reactant velocity fluctuations are very similar. The latter also highlights the good experimental repeatability and accurate control of boundary conditions that is essential for the comparisons with numerical investigations. The enhanced dilation of the $\Phi = 0.70$ case leads to the higher mean axial product fluid velocity and reduced fluctuations close to the reaction onset (i.e. $x/D \simeq 0$). The

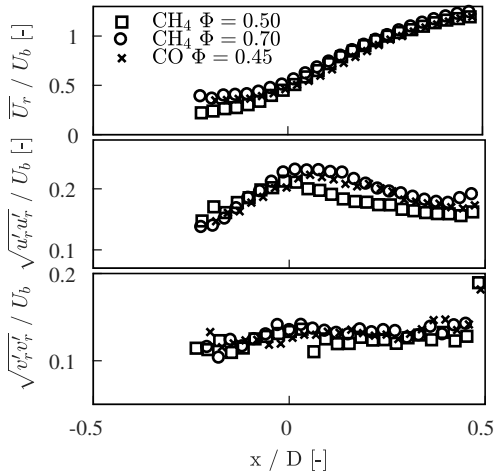

Figure 3: Conditional reactant fluid velocity statistics ($\overline{U}$ mean axial velocity, u' axial fluctuation, v' radial fluctuation) along the stagnation point streamline, normalised by the bulk velocity (U_b), for the 60% H_2 / 40% CH_4 and 60% H_2 / 40% CO mixtures at different equivalence ratios.

60% H_2 / 40% CO at $\Phi = 0.45$ shows conditional reactant and product fluid velocities and fluctuations similar to the $\Phi = 0.70$ mixture with CH_4. This can be attributed to the advanced reaction onset and flame anchoring in low strain regions where dilatation is more effective.

4.2. Turbulent burning velocity

The measured leading edge ($\overline{c} = 0.02$ iso-contour) [21] turbulent burning velocity ($S_{T,l}$) is depicted for all H_2 / CH_4 mixtures in the top panel of Fig. 5 as a function of β. As the amount of CH_4 is increased, a higher equivalence ratio is required to stabilise a self-propagating flame that detaches from the stagnation plane. For example, the pure H_2 / air flame is stabilised at $\Phi = 0.35$ (i.e. upper limit to avoid flashback). A CH_4 blending of 20% and 50% results in a significantly decreased reactivity, a strong reduction of $S_{T,l}$ and increased upper Φ limits of 0.50 and 0.80, respectively. Scaling of $S_{T,l}$ with

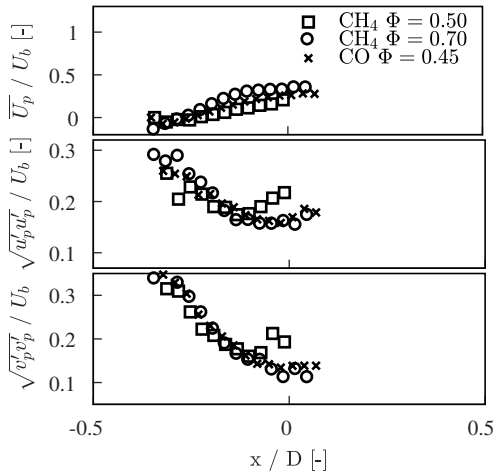

Figure 4: Conditional product fluid velocity statistics ($\overline{U}$ mean axial velocity, u' axial fluctuation, v' radial fluctuation) along the stagnation point streamline, normalised by the bulk velocity (U_b), for the 60% H_2 / 40% CH_4 and 60% H_2 / 40% CO mixtures at different equivalence ratios.

the axial velocity fluctuations collapses the data to $S_{T,l}/\sqrt{u_l'u_l'} = 2.68 \pm 0.19$. By omitting cases that are influenced by the HCP (i.e. grey data points in Fig. 5) the predictive capability of the KPP type velocity in Eq. (5) over the current range is reasonable with $S_{T,l}/S_T^* = 1.16 \pm 0.07$. Scaling the data with the correlations from Peters [39], Bradley *et al.* [38] and Zhang *et al.* [14] result in $S_{T,l}/S_T^\dagger = 2.83 \pm 0.65$, $S_{T,l}/S_T^\ddagger = 1.64 \pm 0.11$, $S_{T,l}/S_T^\# = 1.95 \pm 0.11$, respectively. The KPP derived expression also shows reasonable agreement with $S_{T,l}/S_T^* = 1.24 \pm 0.09$ over the entire H_2 / CO data range. Scaling by $\sqrt{u_l'u_l'}$ results in 2.66 ± 0.20 and the correlations from Peters [39], Bradley *et al.* [38] and Zhang *et al.* [14] result in $S_{T,l}/S_T^\dagger = 3.16 \pm 0.57$, $S_{T,l}/S_T^\ddagger = 1.76 \pm 0.16$, $S_{T,l}/S_T^\# = 2.02 \pm 0.21$, respectively.

The level of disagreement obtained with some of the scalings is not surprising. The opposed jet configuration features an imposed pressure gradient

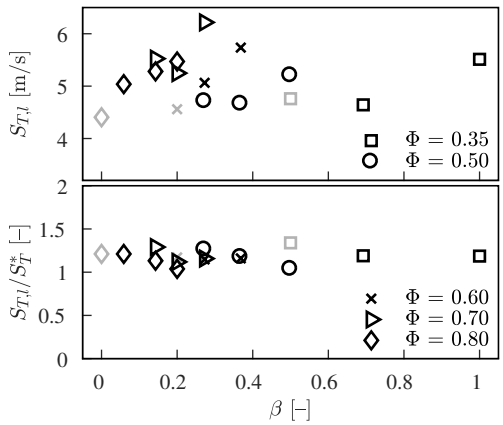

Figure 5: Leading edge turbulent burning velocity ($S_{T,l}$) for H_2 / CH_4 mixtures as a function of β. Top: Measured $S_{T,l}$; Bottom: $S_{T,l}/S_T^*$. The grey symbols indicate thermally supported cases.

and a complex transition between gradient and non-gradient transport. In addition, it has been shown that pressure transport, dilation and scrambling terms play a significant role [47] in the flamelet regime. Furthermore, the observed trend is in agreement with the observations of Laizet and Vassilicos [45] that scalar transport is significantly enhanced by fractal grids. Accordingly, the systematic deviation $\simeq 21\%$ obtained with the KPP derived scaling expression obtained with $Sc_t = 0.7$ appears modest and can be further reduced to $\simeq 10\%$ for $Sc_t = 0.5$.

The influence of CO blending on the mixture reactivity is strongly reduced compared to CH_4, in particular for lean cases as illustrated in Fig. 6. For example, a mixture with $\Phi = 0.35$ can accommodate a 30% CO substitution while maintaining a self-sustained flame. By contrast, a 20% CH_4 substitution results in thermally supported burning. The turbulent burning velocity reduces by ~ 0.02 ms^{-1} per % of CO substitution and approximately twice this value for CH_4 substitution in the range $80 \leq H_2\ (\%) \leq 100$ content.

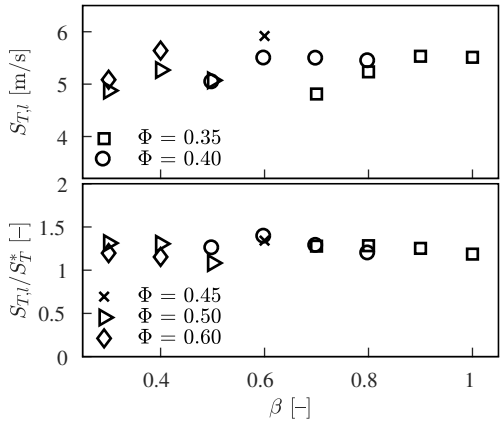

Figure 6: Leading edge turbulent burning velocity ($S_{T,l}$) for H_2 / CO mixtures as a function of β. Top: Measured $S_{T,l}$; Bottom: $S_{T,l}/S_T^*$.

This strong difference is also evident at $\Phi = 0.50$, where $S_{T,l}$ reduces by 0.01 and 0.02 ms^{-1} per percent CO or CH_4 substitution corresponding to a variation from $0.3 \leq \beta \leq 0.5$ for both blends. The strong inhibiting effect of CH_4 on the H_2 reaction chemistry compared to CO was also evident in laminar flames, explosion over pressures and fast turbulent deflagrations [5, 7] as well as auto-ignition in a turbulent shear layer [8].

4.3. Reaction progress conditions

The conditional reactant ($\overline{U_r}$), product ($\overline{U_p}$) and slip velocity ($\overline{U_s}/U_b$) are depicted along with the axial scalar flux ($\overline{c'u'}$) across the turbulent flame brush in Fig. 7 for the 60% H_2 mixture at $\Phi = 0.50$ and 0.70 for CH_4 and $\Phi = 0.45$ for CO. The $\Phi = 0.70$ mixture exhibits a higher $S_{T,l}$, an earlier reaction onset and thus a higher reactant velocity throughout the entire flame brush compared to the leaner mixtures. This leads to a higher product fluid velocity, advanced dilatation and consequently a less negative slip velocity and reduced gradient scalar flux. The reduced inhibiting effect of CO on the

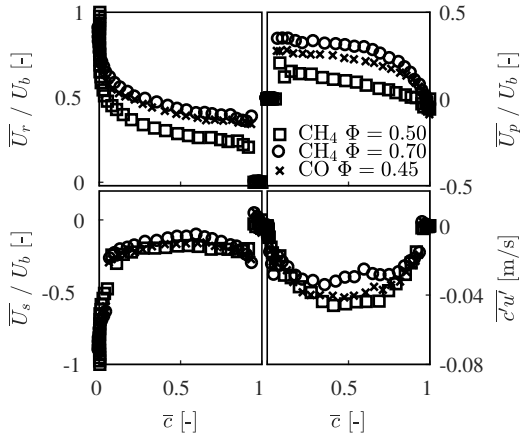

Figure 7: Normalised slip velocity ($\overline{U_s}$) and scalar flux ($\overline{cu}$) as a function of $\overline{c}$ for the mixture 60% H_2 / 40% CH_4 or CO. □ CH_4 $\Phi = 0.50$; ○ CH_4 $\Phi = 0.70$; × CO $\Phi = 0.45$.

H_2 reactivity leads to a reduced gradient scalar flux for the CO ($\Phi = 0.45$) compared to the CH_4 ($\Phi = 0.50$) mixture.

Tian and Lindstedt [47] showed that the product τS_L, where $\tau = (T_{ad} - T_r)/T_r$ is the heat release parameter, scales the pressure transport, dilatation and scrambling terms in the flamelet regime of combustion, while Li *et al.* [5] showed that a normalised scaling based on $(\tau+1)S_L$ can successfully correlate syngas explosion data. The influence of τS_L on the scalar flux conditioned on the $\overline{c} = 0.50$ iso-contour is shown in Fig. 8 for varying H_2 concentration and Φ while maintaining the other parameters constant to quantify their impact. The Φ variation is performed for the 60% H_2 fuel blends in the range $0.50 \leq \Phi \leq 0.70$ for CH_4 and $0.40 \leq \Phi \leq 0.45$ for CO due to the number of available points. For a given lean mixture, an increase in Φ exhibits a two-fold effect that influences the scalar flux: (i) a higher burning velocity due to the elevated mixture reactivity and (ii) an enhanced dilatation due to the higher heat release parameter. For CH_4 / H_2, $S_{T,l}$ increases from 4.7 to

6.2 ms^{-1} and τS_L from 1.4 to 3.0 ms^{-1} with Φ. For CO / H_2, $S_{T,l}$ increases from 5.5 to 5.9 ms^{-1} and τS_L from 1.5 to 2.0 ms^{-1}. The scalar flux in the centre of the turbulent flame brush decreases accordingly (i.e. towards counter-gradient transport) from –0.41 to –0.27 ms^{-1} and –0.48 to –0.37 ms^{-1} with increasing Φ for CH_4 and CO blends, respectively. The H_2 variation for the CH_4 and CO blends is performed at $\Phi = 0.80$ and 0.35, representing the highest and lowest heat release limits. The addition of H_2 to CH_4 / (CO) yields a pronounced / (modest) increase of τS_L of 25×10^{-3} ms^{-1} / (8.7×10^{-3} ms^{-1}) per percent H_2 substitution for the given Φ. Moreover, the measured $S_{T,l}$ increases from 4.4 to 5.5 ms^{-1} by moving from 100% CH_4 to the 50% H_2 / 50% CH_4 fuel blend at $\Phi = 0.80$. Similarly, $S_{T,l}$ increases from 4.8 to 5.5 ms^{-1} by increasing the H_2 content from 70% to 100% in the CO blend at $\Phi = 0.35$. By contrast, $\overline{cu}|(\overline{c} = 0.50)$ decreases significantly with increasing H_2 content for both fuel blends but at a different rate. The transition towards counter-gradient transport is more rapid in CO mixtures where $\overline{cu}|(\overline{c} = 0.50)$ reduces by 0.57 ms^{-1} per unit increase of τS_L (5.7×10^{-3} ms^{-1} per % H_2 increase) in CO blends compared to 0.30 ms^{-1} (8.7×10^{-3} ms^{-1}) in CH_4. The trends are consistent for all conditions with the acceleration across the flame front, as expected, stronger for mixtures with a higher $S_{T,l}$. With increasing reactivity, $\overline{cu}|(\overline{c} = 0.50)$ moves towards counter-gradient transport (i.e. less negative values), yet the transition is suppressed at the current turbulence levels. The stronger inhibiting effect of CH_4 prevails for $\overline{cu}|(\overline{c} = 0.50)$.

The turbulent flow field (i.e. U_b, u_{rms} and Re_t) is maintained constant, yet the rate of the normal compressive strain increases towards the stagnation plane. Selected data are plotted in terms of $S_{T,l}$ as function of the mean

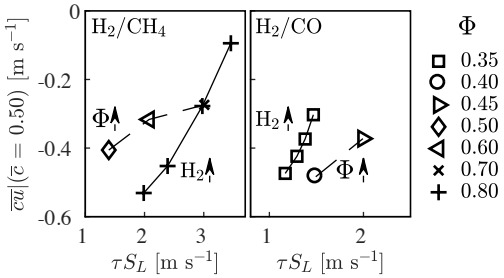

Figure 8: Scalar flux ($\overline{cu}$) conditioned on the $\overline{c} = 0.5$ iso-contour as a function of τS_L for selected data. Left: H_2/CH_4 with 0% – 50% H_2 at $\Phi = 0.80$; $0.50 \leq \Phi \leq 0.70$ at 60% H_2/40% CH_4; Right: H_2/CO with 70% – 100% H_2 at $\Phi = 0.35$; $0.40 \leq \Phi \leq 0.45$ at 60% H_2/40% CO.

normal compressive strain conditioned on the instantaneous flame front ($\overline{a_n}$, see Sec. 3.2) in Fig. 9 to delineate the effect of H_2 addition and Φ separately. An increase in H_2 content from 0 to 50% in CH_4 with $\Phi = 0.80$ ($2.0 \leq \tau S_L$ (ms^{-1}) ≤ 3.5) results in a reduction of $\overline{a_n}$ acting on the flame front from –582 to –39.4 s^{-1}. This is attributed to the increasing detachment of the flame front from the stagnation plane with $S_{T,l}$, i.e. from 4.4 to 5.5 ms^{-1}. The corresponding scalar flux conditioned on the $\overline{c} = 0.50$ iso-contour reduces from –0.53 to –0.09 ms^{-1}.

An increase in Φ (0.50 to 0.70) of the 60% H_2 / CH_4 mixture results in a similar increase of $S_{T,l}$ (4.7 to 6.2 ms^{-1}) and τS_L (1.4 to 3.0 ms^{-1}) and a weaker reduction in $\overline{a_n}$ (–493 to –232 s^{-1}) as well as $\overline{cu}|(\overline{c} = 0.5)$ (–0.41 to –0.28 ms^{-1}). Hydrogen blending to CO (70 to 100% H_2) at $\Phi = 0.35$ causes an increase of $S_{T,l}$ from 4.8 to 5.5 ms^{-1} and a reduced mean normal compressive strain from –473 to –231 s^{-1}. The scalar flux reduces towards counter-gradient transport from –0.47 to –0.34 ms^{-1}. The increase in Φ leads to an increase in $S_{T,l}$ from 5.5 to 5.9 ms^{-1}, $\overline{a_n}$ is reduced from –422 to –291 s^{-1}) and $\overline{cu}|(\overline{c} = 0.5)$ from –0.48 to –0.37 ms^{-1}.

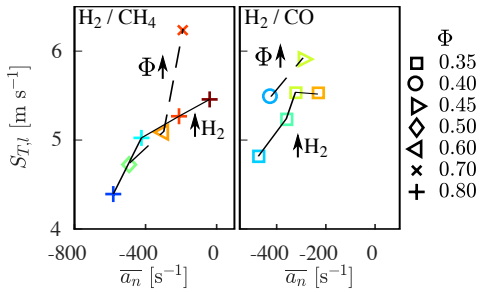

Figure 9: Turbulent burning velocity ($S_{T,l}$) vs the mean normal compressive strain acting on the flame front ($\overline{a_n}$). Left: H_2/CH_4 with $0\% \leq H_2 \leq 50\%$ at $\Phi = 0.80$; $0.50 \leq \Phi \leq 0.70$ at 40% CH_4; Right: H_2/CO with $70\% \leq H_2 \leq 100\%$ in CO at $\Phi = 0.35$; $0.40 \leq \Phi \leq 0.45$ at 40% CO. The symbol colour blue to red indicates $\overline{cu}|(\overline{c} = 0.50)$, i.e. gradient towards counter-gradient transport.

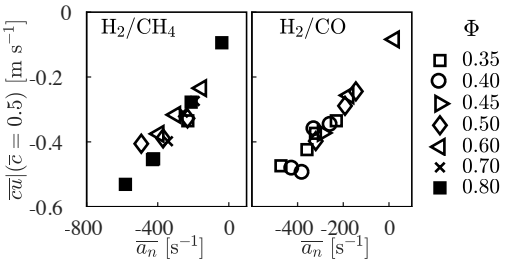

Figure 10: Scalar flux conditioned at the centre of the turbulent flame brush ($\overline{cu}|(\overline{c} = 0.5)$) as a function of mean normal compressive strain acting on the flame front ($\overline{a_n}$). Top left: H_2 / CH_4; Right: H_2 / CO.

The correlation between the mean normal compressive strain and scalar flux conditioned on ($\overline{c} = 0.50$) is depicted in Fig. 10 for all data points. The data are very well correlated with linear regression coefficients (R^2) of 0.93 and 0.95 for H_2 / CH_4 and H_2 / CO, respectively. Consequently, scalar transport is strongly influenced by the total rate of strain strain.

5. Conclusions

The present study has quantified the impact of the reactivity of hydrogen enriched fuel blends, e.g. syngas, on turbulence–chemistry interactions and scalar transport utilising a back-to-burnt opposed jet configuration for aerodynamic flame stabilisation. The turbulent flow field ($Re_t = 314 \pm 19$) and the burnt gas state temperature ($T_{HCP} = 1640 \pm 7$ K) are maintained constant to delineate chemistry effects of binary H_2 / CH_4 and H_2 / CO fuel blends. The H_2 content is varied from pure CH_4 to 100% H_2 and from 30 to 100% H_2 in CO blends. The equivalence ratio is adjusted between the mixture specific lower limit of local flame extinction and the upper limit of flashback. An increase in mixture reactivity results in a higher turbulent burning velocity. Methane exhibits a stronger pronounced inhibiting effect on the hydrogen chemistry compared to carbon monoxide with the β scaling attenuating the differences. The KPP-type approach predicts the measured $S_{T,l}$ within 21 ± 9% for all self-sustained flames. A distinct transition towards counter-gradient transport with increasing $S_{T,l}$ and thermal expansion ratio is established and influenced by the rate of compressive strain. Thus, mixtures with a high $S_{T,l}$ detach further from the stagnation plane and anchor in low compressive strain regions where dilatation is more effective and lead to a transition towards counter-gradient transport. The transition is suppressed by the high turbulence levels. This is supported by a correlation coefficient (R^2) > 0.93 for the scalar flux conditioned on the centre of the turbulent flame brush as a function of mean normal compressive strain ($\overline{a_n}$) acting on the flame front. The correlation $S_{T,l}$ – $\overline{a_n}$ also shows a reasonable correlation. The results provide guidance to engine manufacturers and

inform risk assessments as to the use of hydrogen enriched mixtures. The wide range of conditions further presents an excellent challenge for turbulent combustion models that aim to delineate the influence of fuel reactivity.

Acknowledgements

The authors gratefully acknowledge the financial support of the ETI under the High Hydrogen project (PE02162) and Dr Robert Barlow of Sandia National Laboratories and Prof. Hans Michels of Imperial College.

References

[1] T. Lieuwen, V. Yang, R. Yetter (eds.) Synthesis Gas Combustion, Boca Raton: CRC Press, 2009.

[2] S. Daniele, P. Jansohn, J. Mantzaras, K. Boulouchos, Turbulent flame speed for syngas at gas turbine relevant conditions, Proc. Comb. Inst. 33 (2011), 2937–2944.

[3] B. Korb, S. Kawauchi, G. Wachtmeister, Influence of hydrogen addition on the operating range, emissions and efficiency in lean burn natural gas engines at high specific loads, Fuel 164 (2016), 410–418.

[4] T. Lieuwen, V. McDonell, D. Santavicca, T. Sattelmayer, Burner Development and Operability Issues Associated with Steady Flowing Syngas Fired Combustors, Comb. Sci. Technol. 180 (2008), 1169–1192.

[5] T. Li, F. Hampp, R. P. Lindstedt, Turbulent explosions in hydrogen enriched syngas related fuel blends, Process Saf. Environ. 116 (2018), 663–676.

[6] C. K. Law, G. Jomaas, J. K. Bechtold, Cellular instabilities of expanding hydrogen/propane spherical flames at elevated pressures: theory and experiment, Proc. Combust. Inst. 30 (2005), 159–167.

[7] T. Li, F. Hampp, R. P. Lindstedt, The impact of hydrogen enrichment on the flow field evolution in turbulent explosions, Combust. Flame (2018), 105–119.

[8] P. Simatos, F. Hampp, R. P. Lindstedt, in A. Runchal, A. Gupta, A. Kushari, A. De, S. Aggarwal (eds.), Innovations in Sustainable Energy and Cleaner Environment, Springer-Nature, Singapore (2018).

[9] Y.-C. Lin, S. Daniele, P. Jansohn, K. Boulouchos, Turbulent Flame Speed as an Indicator for Flashback Propensity of Hydrogen-Rich Fuel Gases, J. Eng. Gas Turbines Power 135 (2013) 111503.

[10] E. M. Burke, F. Güthe, R. F. D. Monaghan, A comparison of turbulent flame speed correlations for hydrocarbon fuels at elevated pressures, Proc. ASME Turbo Expo, Seoul, South Korea (2016) GT2016-57804.

[11] J. Wang, M. Zhang, Y. Xie, Z. Huang, T. Kudo, H. Kobayashi, Correlation of turbulent burning velocity for syngas/air mixtures at high pressure up to 1.0 MPa, Exp. Thermal Fluid Sci. 50 (2013) 90–96.

[12] P. Venkateswaran, A. D. Marshall, J. M. Seitzman, T. C. Lieuwen, Turbulent Consumption Speeds of High Hydrogen Content Fuels From 1-20 atm, J. Eng. Gas Turb. Power, 136 (2013) 011504.

[13] S. S. Shy, C. C. Liu, J. Y. Lin, L. L. Chen, A. N. Lipatnikov, S. I. Yang,

Correlations of high-pressure lean methane and syngas turbulent burning velocities: Effects of turbulent Reynolds, Damköhler, and Karlovitz numbers, Proc. Combust. Inst. 35 (2015), 1509–1506.

[14] W. Zhang, J. Wang, Q. Yu, W. Jin, M. Zhang, Z. Huang, Investigation of the fuel effects on burning velocity and flame structure of turbulent premixed flames based on leading points concept, Combust. Sci. Technol. 190 (2018), 1354–1376.

[15] S. Daniele, P. Jansohn, K. Boulouchos, Flame front characteristic and turbulent flame speed of lean premixed syngas combustion at gas turbine relevant conditions, Proc. ASME Turbo Expo, Orlando, Florida, USA (2009) GT2009-59477.

[16] S. P. R. Muppala, M. Nakahara, N. K. Aluri, H. Kido, J. X. Wen, M. V. Papalexandris, Experimental and analytical investigation of the turbulent burning velocity of two-component fuel mixtures of hydrogen, methane and propane, Int. J. Hyd. Energ. 34 (2009), 9258–9265.

[17] C. C. Liu, S. S. Shy, C. W. Chiu, M. W. Peng, H. J. Chung, Hydrogen/carbon monoxide syngas burning rates measurements in high-pressure quiescent and turbulent environment, Int. J. Hyd. Energ. 36 (2011), 8595–8603.

[18] K. N. C. Bray, Studies of the turbulent burning velocity, Proc. R. Soc. A 431 (1990), 315–335

[19] J. F. Driscoll, Turbulent premixed combustion: Flamelet structure and

its effect on turbulent burning velocities, Prog. Energy Combust. Sci. 34 (2008), 91–134.

[20] I. G. Shepherd, R. K. Cheng, The burning rate of premixed flames in moderate and intense turbulence, Combust. Flame, 127 (3) (2001), 2066–2075

[21] C. J. Lawn, R. W. Schefer, Scaling of premixed turbulent flames in the corrugated regime, Combust. Flame 146 (2006), 180–199.

[22] K. H. H. Goh, P. Geipel, F. Hampp, R. P. Lindstedt, Flames in fractal grid generated turbulence, Fluid Dyn. Res. 45, (2013), 061403.

[23] K. H. H. Goh, P. Geipel, R. P. Lindstedt, Lean premixed opposed jet flames in fractal grid generated multiscale turbulence, Combust. Flame 161 (2014), 2419–2434.

[24] F. Hampp, R.P. Lindstedt, Quantification of combustion regime transitions in premixed turbulent DME flames, Combust. Flame 182 (2017), 248–268.

[25] K. H. H. Goh, P. Geipel, F. Hampp, R. P. Lindstedt, Regime transition from premixed to flameless oxidation in turbulent JP-10 flames, Proc. Combust. Inst. 34 (2013), 3311–3318.

[26] P. Geipel, K. H. H. Goh, R. P. Lindstedt, Fractal-Generated Turbulence in Opposed Jet Flows, Flow Turbul. Combust. 85 (2010), 397–419.

[27] D. Geyer, A. Kempf, A. Dreizler, J. Janicka, Turbulent opposed-jet

flames: A critical benchmark experiment for combustion LES, Combust. Flame 143 (2005), 524–548.

[28] E. Mastorakos, A. M. K. P. Taylor, J. H. Whitelaw, Extinction of Turbulent Counterflow Flames with Reactants Diluted by Hot Products, Combust. Flame 102 (1995), 101–114.

[29] F. Hampp, R. P. Lindstedt, Strain distribution on material surfaces during combustion regime transitions, Proc. Combust. Inst. 36 (2017), 1911–1918.

[30] F. Hampp, S. Shariatmadar, R. P. Lindstedt, Quantification of low Damköhler number turbulent premixed flames, Proc. Combust. Inst. (2018), 2373–2381.

[31] F. Hampp, R. P. Lindstedt, in A. Runchal, A. Gupta, A. Kushari, A. De, S. Aggarwal (eds.), Energy for Propulsion, Green Energy and Technology Series, Springer-Nature, Singapore (2018).

[32] F. Hampp, R. P. Lindstedt, in Y. Sakai and C. Vassilicos (eds.) Fractal Flow Design: How to Design Bespoke Turbulence and why, Springer-Verlag, CISM Int. Mech. Sci. 568 (2016).

[33] I. G. Shepherd, R. K. Cheng, P. J. Goix, The spatial scalar structure of premixed turbulent stagnation point flames, Proc. Combust. Inst. 23 (1991), 781–787.

[34] K. N. C. Bray, in N. Swaminathan, K. N. C. Bray (eds.), Turbulent Premixed Flames, Cambridge University Press (2001), 41–60.

[35] D. B. Spalding, Mixing and chemical reaction in steady confined turbulent flames, Proc. Combust. Inst. 13 (1971), 649–657.

[36] B. Hakberg, A. D. Gosman, Analytical determination of turbulent flame speed from combustion models, Proc. Combust. Inst. 20 (1985), 225–232.

[37] C. A. Catlin, R. P. Lindstedt, Premixed turbulent burning velocities derived from mixing controlled reaction models with cold front quenching, Combust. Flame 85 (1991), 427–439.

[38] D. Bradley, A. K. C. Lau, M. Lawes, Flame stretch rate as a determinant of turbulent burning velocity, Philos. Trans. R. Soc. A: Math. Phys. Eng. Sci. 338 (1992), 359–387.

[39] N. Peters, The turbulent burning velocity for large-scale and small-scale turbulence, J. Fluid Mech. 384 (1999), 107–132.

[40] R. P. Lindstedt, V. Sakthitharan, Modelling of transient compressible turbulent reacting flows, in: 8th Symposium on Turbulent Shear Flows, 1991.

[41] A. N. Kolmogorov, I. G. Petrovskii, N. S. Piskunov, A study of the diffusion equation with increase in the amount of substance, and its application to a biological problem, Bull. Moscow Univ. Math. Mech. 1 (1937), 1–26.

[42] R. P. Lindstedt, E. M. Váos, Modeling of premixed turbulent flames with second moment methods, Combust. Flame 116 (1999), 461–485.

[43] N. K. Aluri, S. P. Reddy Muppala, F. Dinkelacker, Substantiating a fractal-based algebraic reaction closure of premixed turbulent combustion for high pressure and the Lewis number effects, Combust. Flame 145 (2006), 663–674.

[44] C. Gualtieri, A. Angeloudis, F. Bombardelli, S. Jha and T. Stoesser, On the Values for the Turbulent Schmidt Number in Environmental Flows, Fluids 2 (2017), 17.

[45] S. Laizet, J. C. Vassilicos, Fractal space-scale unfolding mechanism for energy-efficient turbulent mixing, Phys. Rev. E 86 (2012), 046302.

[46] R. P. Lindstedt, V. D. Milosavljevic, M. Persson, Turbulent burning velocity predictions using transported pdf methods, Proc. Combust. Inst. 33 (2011), 1277–1284.

[47] L. Tian, R. P. Lindstedt, The impact of dilatation, scrambling and pressure transport in turbulent premixed flames, Combust. Theory Model. 21 (2017) 1114–1147.

Table 1: Data summary of H_2 / CH_4 and H_2/CO mixtures, where β is defined in Eq. (1), Φ is the equivalence ratio, ρ_r the density of the reactants (r), ν_r the kinematic viscosity, Le_r the Lewis number, $\tau = (T_{ad} - T_r)/T_r$ the heat release parameter, $S_{L,0}$ and S_L the unstrained and strained laminar burning velocity, δ_f the laminar flame thickness and a_q the laminar rate of strain at extinction.

Mixture	β	Φ	ρ_r	$\nu_r \times 10^{-5}$	Le_r	τ	$S_{L,0}$	S_L	δ_f	a_q
H_2 / CH_4	[-]	[-]	[kg/m^3]	[m^2/s]	[-]	[-]	[m/s]	[m/s]	[mm]	[s^{-1}]
100%/0%	1.0	0.35	1.04	1.78	0.374	3.33	0.076	0.44	1.19	3600
90%/10%	0.69	0.35	1.08	1.71	0.438	3.22	0.032	0.33	2.59	2000
80%/20%	0.50	0.35	1.10	1.68	0.500	3.13	0.016	0.26	4.42	800
80%/20%	0.50	0.50	1.07	1.72	0.527	4.10	0.164	0.52	0.703	4000
70%/30%	0.37	0.50	1.09	1.68	0.585	4.04	0.121	0.39	0.821	2400
70%/30%	0.37	0.60	1.07	1.70	0.600	4.55	0.240	0.55	0.515	4300
60%/40%	0.27	0.50	1.10	1.66	0.641	3.99	0.096	0.35	0.971	1400
60%/40%	0.27	0.60	1.09	1.67	0.654	4.52	0.194	0.46	0.588	2900
60%/40%	0.27	0.70	1.08	1.69	0.666	4.93	0.308	0.61	0.436	4300
50%/50%	0.20	0.60	1.11	1.65	0.707	4.49	0.164	0.39	0.651	1900
50%/50%	0.20	0.70	1.09	1.66	0.717	4.91	0.263	0.52	0.480	3100
50%/50%	0.20	0.80	1.08	1.67	0.727	5.24	0.364	0.66	0.393	4000
40%/60%	0.14	0.70	1.11	1.64	0.768	4.89	0.231	0.46	0.517	2300
40%/60%	0.14	0.80	1.10	1.65	0.775	5.22	0.322	0.57	0.420	3000
20%/80%	0.06	0.80	1.12	1.61	0.869	5.19	0.267	0.46	0.468	1900
0% /100%	0.00	0.80	1.14	1.58	0.962	5.09	0.228	0.39	0.511	1300
H_2 / CO										
100%/0%	1.0	0.35	1.04	1.78	0.374	3.34	0.077	0.44	1.19	3600
90%/10%	0.90	0.35	1.05	1.75	0.467	3.37	0.072	0.41	1.25	3500
80%/20%	0.80	0.35	1.07	1.73	0.554	3.40	0.069	0.38	1.31	2700
80%/20%	0.80	0.40	1.05	1.75	0.567	3.76	0.142	0.47	0.786	4200
70%/30%	0.70	0.35	1.08	1.71	0.635	3.44	0.065	0.34	1.37	1900
70%/30%	0.70	0.40	1.07	1.73	0.648	3.80	0.130	0.43	0.839	3200
60%/40%	0.60	0.40	1.08	1.70	0.722	3.83	0.120	0.39	0.895	2300
60%/40%	0.60	0.45	1.07	1.72	0.734	4.15	0.191	0.48	0.672	3500
50%/50%	0.50	0.40	1.10	1.68	0.788	3.87	0.110	0.35	0.955	1600
50%/50%	0.50	0.45	1.09	1.69	0.800	4.19	0.173	0.43	0.724	2500
50%/50%	0.50	0.50	1.08	1.70	0.811	4.48	0.246	0.52	0.596	3500
40%/60%	0.40	0.50	1.10	1.67	0.866	4.51	0.219	0.46	0.646	2500
40%/60%	0.40	0.60	1.09	1.69	0.883	4.97	0.366	0.63	0.508	4200
30%/70%	0.30	0.50	1.12	1.65	0.911	4.54	0.193	0.39	0.708	1700
30%/70%	0.30	0.60	1.11	1.66	0.924	5.00	0.319	0.56	0.556	2900

Table 2: Result summary for H_2 / CH_4 and H_2 / CO fuel mixtures, where Φ_{UN} is the upper nozzle equivalence ratio, Re_t the turbulent Reynolds number, Da the Damköhler number, u'_r the axial reactant velocity fluctuation at the nozzle exit, u'_l the axial velocity fluctuation at the leading edge ($\overline{c} = 0.02$ iso-contour), $\widehat{u}'$ the maximum axial velocity fluctuation in the flame brush, $\overline{u_t}$ the mean velocity at the trailing edge ($\overline{c} = 0.95$ iso-contour), $S_{T,l}$ the measured turbulent burning velocity at the leading edge ($\overline{c} = 0.02$ iso-contour) and S_T^* is the KPP-type turbulent burning velocity).

Mixture	Φ_{UN}	Re_t	Da	u'_r	u'_l	$\widehat{u}'$	$\overline{u_t}$	$S_{T,l}$	S_T^*
H_2 / CH_4	[-]	[-]	[-]	[m/s]	[m/s]	[m/s]	[m/s]	[m/s]	[m/s]
100%/0%	0.35	307	1.03	1.60	1.87	1.96	0.846	5.51	4.65
90%/10%	0.35	294	0.384	1.47	1.88	1.96	0.154	4.64	3.90
80%/20%	0.35	339	0.157	1.68	2.01	2.19	-0.0880	4.76	3.55
80%/20%	0.50	314	2.09	1.61	1.98	1.99	0.669	5.20	5.03
70%/30%	0.50	299	1.44	1.48	1.87	1.97	0.169	4.66	3.97
70%/30%	0.60	302	3.13	1.55	1.94	1.98	1.11	5.74	4.95
60%/40%	0.50	300	1.11	1.47	1.91	2.04	0.0056	4.71	3.74
60%/40%	0.60	320	2.22	1.63	1.96	1.98	0.338	5.06	4.41
60%/40%	0.70	334	3.74	1.71	2.07	2.13	0.545	6.22	5.37
50%/50%	0.60	315	1.76	1.49	1.93	2.01	-0.0114	4.56	3.89
50%/50%	0.70	310	3.20	1.59	2.01	2.04	0.585	5.25	4.69
50%/50%	0.80	302	5.11	1.48	1.98	1.98	1.58	5.47	5.27
40%/60%	0.70	321	2.56	1.58	2.00	2.02	0.124	5.52	4.28
40%/60%	0.80	317	3.96	1.52	1.93	2.00	0.722	5.28	4.66
20%/80%	0.80	327	2.83	1.56	2.03	2.09	0.164	5.04	4.16
0% /100%	0.80	324	2.27	1.51	2.03	2.17	-0.0145	4.41	3.64
H_2 / CO									
100%/0%	0.35	307	1.03	1.60	1.87	1.96	0.846	5.51	4.85
90%/10%	0.35	289	0.985	1.48	1.93	2.01	0.413	5.53	4.42
80%/20%	0.35	306	0.833	1.54	1.93	1.96	0.266	5.23	4.08
80%/20%	0.40	303	1.70	1.52	1.93	1.97	0.713	5.43	4.56
70%/30%	0.35	307	0.719	1.50	1.96	1.99	0.0462	4.81	3.77
70%/30%	0.40	314	1.44	1.51	1.98	2.06	0.435	5.48	4.29
60%/40%	0.40	323	1.20	1.56	1.99	2.10	0.193	5.48	3.96
60%/40%	0.45	313	2.03	1.54	1.99	2.08	0.544	5.92	4.41
50%/50%	0.40	381	0.876	1.95	2.23	2.24	0.0958	5.03	4.02
50%/50%	0.50	358	2.16	1.88	2.11	2.13	1.67	5.07	4.68
40%/60%	0.50	347	1.85	1.81	1.97	2.08	1.56	5.27	4.04
40%/60%	0.60	338	3.29	1.75	2.03	2.04	3.33	5.64	4.89
30%/70%	0.50	342	1.48	1.72	2.03	2.05	0.465	4.88	3.71
30%/70%	0.60	332	2.76	1.66	1.89	1.97	1.47	5.08	4.24